Supporting Information for "Solid-liquid Thermal Transport and its Relationship with Wettability and the Interfacial Liquid Structure"

Bladimir Ramos-Alvarado, Satish Kumar, and G. P. Peterson

The George W. Woodruff School of Mechanical Engineering, Georgia Institute of Technology, Atlanta, Georgia, USA.

Interfacial thermal transport was investigated in silicon and graphene-coated silicon surfaces in contact with water while varying the wettability of the silicon surfaces as indicated in Table S1. The configuration of the systems investigated is depicted in Fig. 1 in the text, where two solid slabs were used to enclose a water block modeled using the SPC/E model[1]. The rigidity of the water molecule was enforce using the SHAKE[2] algorithm and the electrostatic interactions were handled using the PPPM[3] with an accuracy of 1×10^{-6}. The outermost solid atoms were kept fixed in order to enforce a constant volume in the system, while periodic boundary conditions were imposed in the remaining directions. The water-solid non-bonded interactions were modeled using a truncated Lennard-Jones potential where, σ_{CO} = 3.19 Å, ε_{CO} = 0.4736 kJ/mol, and the potential cut-off was 15 Å[4]. These parameters were calibrated to obtain a contact angle of 64.4° on a clean graphite surface[5]. The potential parameters for water-silicon were: σ_{SiO} = 2.635 Å and ε_{SiO} was varied in order to obtain different contact angles, see Table S1. The Si-Si and C-C interactions were modeled using Tersoff potentials[6-7] and the Si-C interactions were accounted for using σ_{SiC} = 2.1 Å, ε_{SiC} = 0.96 kJ/mol in order to bring the graphene layer to an equilibrium distance of ~2 Å from the silicon surface[8-10].

The length of the silicon slabs was 10 nm and that of the water confinement 6 nm, the area of the Si(100) system was 2.7×2.2 nm and that of Si(111) was 3.1×2.7 nm. The different dimensions of the silicon structures were necessary in order to create a periodic structure matching the honeycomb structure of graphene. Graphene was stretched no more than 4%, as previously reported to create a periodic structure[11]. The number of water molecules inside the confinement was varied depending on the wettability conditions so that similar bulk density and pressure were obtained for every system in order to eliminate any pressure effects[12-13]. The simulations were carried out using the MD code LAMMPS[14] and VMD[15] for visualization. The simulation process was as follows: 1) energy minimization of the entire system in order to eliminate any excess potential energy from the initial configuration, 2) equilibration at a constant temperature of 300 K for 1.5 ns using a Nose-Hover thermostat[16-17] with a time constant of 0.1 ps, 3) run in the microcanonical ensemble (NVE) for 1.5 ns in order to verify the stability of the system's temperature without having any thermostat, 4) thermal energy addition/removal at a fixed rate of 2.5-20 nw (depending on the system's wettability) during 2 ns in order to induce a steady state temperature profile in the system, and 5) data sampling of the kinetic energy and coordinates of the atoms every 10 ps during a production run of 6 ns. The temperature profiles of the solid slabs were obtained by time-averaging the kinetic energy (KE) per atomic plane where $T = \mathrm{KE}/1.5k_B$. The temperature profile of the water slab was obtained by means of time-averaging and particle-count averaging the kinetic energy per bin in which the water slab was divided. A total of 50 slabs were used to discretize the 6 nm slab of water, a number large enough to capture the sharp details of the liquid layering near the walls and small enough to avoid a noisy sampling of space. For water $T = \mathrm{KE}/3k_B$, since the rigid SPC/E water model has only 6 degrees of freedom. A sample of the temperature profiles obtained from the simulations is

depicted in Fig. S1. The temperature jump at the interface was determined by extrapolating the linearly-fitted temperature profiles of the phases. It is worth mentioning that the thermal conductivity of water was k_{H2O} = 0.82 ± 0.08 W/m K, a value consistent with the expected conductivity of SPC/E water[18].

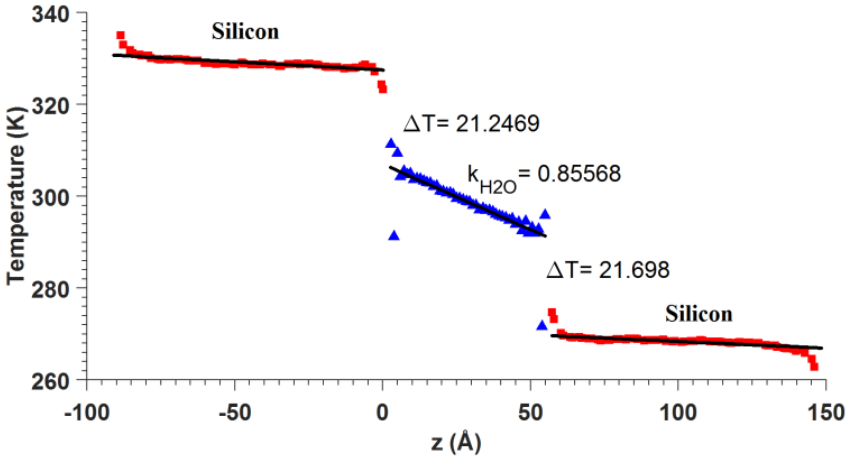

Figure S1. Calculation of the interface temperature jump by means of profiling the temperature in the heat flux direction.

Table S1. Silicon-oxygen interaction potentials and contact angles calculated on Si(100) and Si(111) surfaces.

Si(100)		Si(111)	
ε_{SiO} (kJ/mol)	θ (deg)	ε_{SiO} (kJ/mol)	θ (deg)
2.3328	45.7934°±0.9973°	2.0352	45.3304°±0.282°
2.2368	54.9135±0.2512°	1.9584	47.1844°±0.7544°
2.1408	59.5705°±0.5706°	1.8528	61.2929°±0.2205°
2.0256	68.8011°±0.4501°	1.6128	79.6101°±0.2502°
1.9296	73.8920°±0.4875°	1.5456	83.4333°±0.3515°
1.488	100.8899°±0.3135°	1.2672	101.2268°±0.3082°
1.0656	122.6588°±1.1538°	0.8928	123.5903°±0.5476°
0.624	147.4587°±0.0.4874°	0.5280	153.0708°±0.4762°

The thermal boundary conductance G was calculated as the slope of the curve fitting $J = G\Delta T_{int}$, where J is the heat flux and ΔT_{int} is the temperature jump at the interface. As it can be observed in Fig. S1, there is a "hot" wall on the heat input side and a "cold" wall on the heat output side. A linear relationship was obtained for J and ΔT_{int} confirming that this investigation was conducted in the linear response regime. It was consistently observed that $G_{HOT}/G_{COLD} > 1$, as expected. The ratio of the thermal conductance of the hot to the cold wall is reported in Fig. S2. The results indicate that in most of the cases, the G values are very similar between hot and cold walls. Fig. S2 also shows that G_{HOT}/G_{COLD} is smaller for the Si(100) system than for Si(111), this is due to the liquid interfacial structure effects and phonons density of states variations between both systems as explained in the main text.

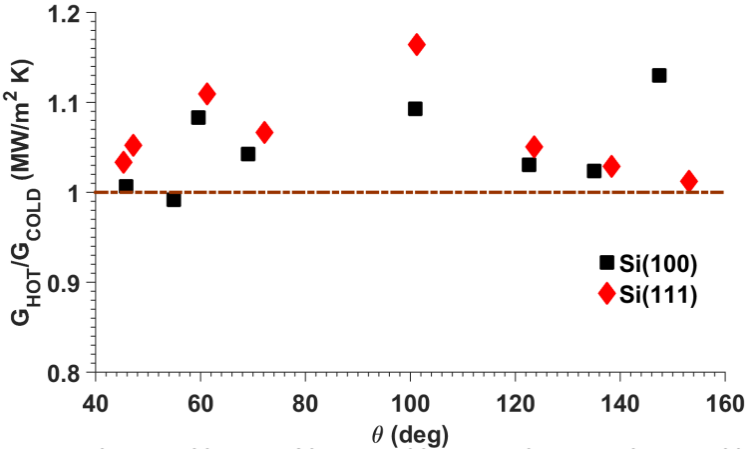

Figure S2. Ratio of the hot and cold thermal boundary conductance calculations for different wettability conditions.

Figure S3 reports on the dependence of G of on the silicon-water interaction strength. As expected, the thermal transport is more effective if the solid-liquid interaction is stronger. However, there is still a lack of generality in the behavior of the different silicon surfaces, since the Si(100) surface keeps appearing as the one with better thermal transport properties.

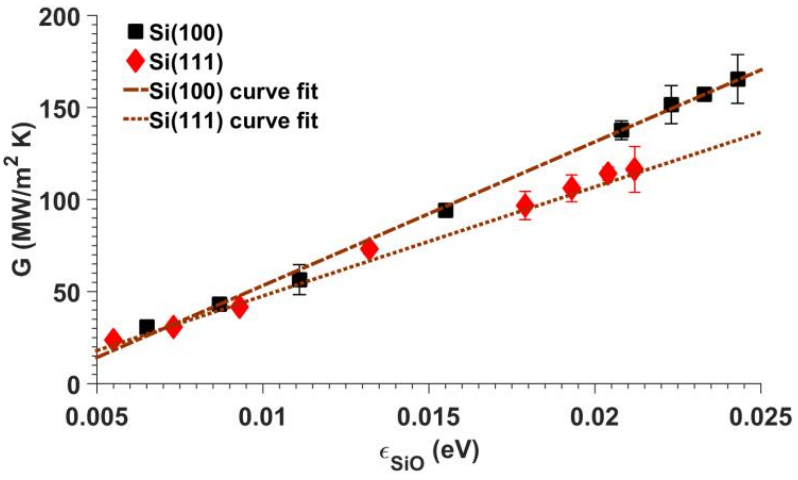

Figure S3. Thermal boundary conductance dependence on the silicon-water interaction strength.

Figure S4 illustrates the characteristics of the interfacial liquid structure. Figure S4(a) depicts the density liquid layering observed in the different silicon and graphene-coated silicon surfaces investigated. The density depletion can be observed at the interface (z = 0) as a region of zero or low density in comparison with the bulk and density peaks. The rest of the Figs. S4 (b), (c), and (d) depict snapshots of the interfacial water for the different surfaces having similar wettability conditions.

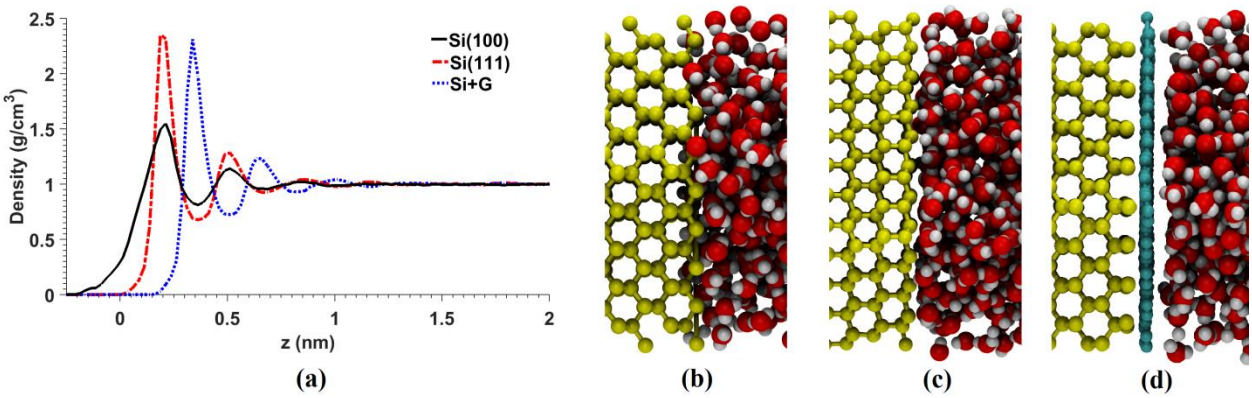

Figure S4. (a) Density layering and snapshots of the interfaces of (b) Si(100), (c) Si(111), and Si(100) coated with graphene under the same wettability conditions, θ = 71°.

References

(1) Berendsen, H. J. C.; Grigera, J. R.; Straatsma, T. P., The Missing Term in Effective Pair Potentials. *J. Phys. Chem.* **1987,** *91* (24), 6269-6271.

(2) Ryckaert, J.-P.; Ciccotti, G.; Berendsen, H. J. C., Numerical Integration of the Cartesian Equations of Motion of a System with Constraints: Molecular Dynamics of n-Alkanes. *J. Comput. Phys.* **1977,** *23* (3), 327-341.

(3) Hockney, R. W.; Eastwood, J. W., *Computer Simulation Using Particles*. Taylor & Francis: New York, NY, 1988.

(4) Ramos-Alvarado, B.; Kumar, S.; Peterson, G. P., Wettability of Graphitic-Carbon and Silicon Surfaces: MD Modeling and Theoretical Analysis. *J. Chem. Phys.* **2015,** *143* (4), 044703.

(5) Li, Z. T.; Wang, Y. J.; Kozbial, A.; Shenoy, G.; Zhou, F.; McGinley, R.; Ireland, P.; Morganstein, B.; Kunkel, A.; Surwade, S. P.; Li, L.; Liu, H. T., Effect of Airborne Contaminants on the Wettability of Supported Graphene and Graphite. *Nat. Mater.* **2013,** *12* (10), 925-931.

(6) Tersoff, J., Empirical Interatomic Potential for Silicon with Improved Elastic Properties. *Phys Rev B* **1988,** *38* (14), 9902-9905.

(7) Tersoff, J., Modeling Solid-State Chemistry - Interatomic Potentials for Multicomponent Systems. *Phys Rev B* **1989,** *39* (8), 5566-5568.

(8) Hackley, J.; Ali, D.; DiPasquale, J.; Demaree, J. D.; Richardson, C. J. K., Graphitic Carbon Growth on Si(111) Using Solid Source Molecular Beam Epitaxy. *App. Phys. Lett.* **2009,** *95* (13), 133114.

(9) Ochedowski, O.; Begall, G.; Scheuschner, N.; El Kharrazi, M.; Maultzsch, J.; Schleberger, M., Graphene on Si(111)7x7. *Nanotechnology* **2012,** *23* (40), 405708.

(10) Tayran, C.; Zhu, Z.; Baldoni, M.; Selli, D.; Seifert, G.; Tománek, D., Optimizing Electronic Structure and Quantum Transport at the Graphene-Si(111) Interface: An ab-initio Density-Functional Study. *Phys. Rev. Lett.* **2013,** *110* (17), 176805.

(11) Ramos-Alvarado, B.; Kumar, S.; Peterson, G. P., On the Wettability Transparency of Graphene-Coated Silicon Surfaces. *J. Chem. Phys.* **2016,** *144* (1), 014701.

(12) Ramos-Alvarado, B.; Kumar, S.; Peterson, G. P., Hydrodynamic Slip in Silicon Nanochannels. *Phys. Rev. E* **2016,** *93* (3), 033117.

(13) Ramos-Alvarado, B.; Kumar, S.; Peterson, G. P., Hydrodynamic Slip Length as a Surface Property. *Phys. Rev. E* **2016,** *93* (2), 023101.

(14) Plimpton, S., Fast Parallel Algorithms for Short-Range Molecular-Dynamics. *J. Comput. Phys.* **1995,** *117* (1), 1-19.

(15) Humphrey, W.; Dalke, A.; Schulten, K., VMD: Visual Molecular Dynamics. *J. Mol. Graph. Model.* **1996,** *14* (1), 33-38.

(16) Nose, S., A Molecular-Dynamics Method for Simulations in the Canonical Ensemble. *Mol. Phys.* **1984,** *52* (2), 255-268.

(17) Hoover, W. G., Canonical Dynamics - Equilibrium Phase-Space Distributions. *Phys. Rev. A* **1985,** *31* (3), 1695-1697.

(18) Sirk, T. W.; Moore, S.; Brown, E. F., Characteristics of Thermal Conductivity in Classical Water Models. *J. Chem. Phys.* **2013,** *138* (6), 064505.